DOI: 10.1002/cnma.201500188

2D Materials | *Very Important Paper*

VIP

SPECIAL ISSUE

Generalized Synthesis of Hierarchical Transition Metal Dichalcogenide Nanosheets from Polyoxometalates

Peilei He, Haoyi Li, Huiling Liu, and Xun Wang*[a]

Abstract: Transition metal dichalcogenides (TMDs, such as MoS_2, WS_2 and $MoSe_2$) with lamellar structures have attracted tremendous attention owing to their similar structure to graphite. However, two-dimensional (2D) TMD nanomaterials display a strong tendency to restack and condense, which leads to a marked decrease of performance in their applications. In this study, we report the synthesis of TMDs by using polyoxometalates (POMs) as tungsten or molybdenum precursors. Hierarchical TMDs with novel structures can be formed below 200 °C, including WS_2 rods, MoS_2 rods and $MoSe_2$ hollow spheres. All of these structures assembled from the corresponding nanosheets. Meanwhile the epitaxial growth of noble metal nanoparticles (NPs) on TMDs could be achieved very easily. The obtained Pt/WS_2 and Pt/MoS_2 hybrids were highly active and durable HER catalysts. In addition, the Pt NPs on the surface of TMDs could improve the HER activity sharply, which was likely due to the synergistic effect between Pt NPs and MoS_2 rods.

Graphene, a two-dimensional (2D) nanomaterial, has been studied for several years because of its potential applications in electronic devices,[1] energy storage,[2] and polymer composites.[3] The rapid developments in graphene research and the special characteristics of graphene, such as the absence of a bandgap,[4] have led to a search for other 2D nanomaterials of inorganic analogues.[5] In particular, transition metal dichalcogenides (TMDs, such as MoS_2, WS_2, and $MoSe_2$) with lamellar structures have attracted tremendous attention owing to the similar structure to graphite and sizable bandgaps.[5,6] Furthermore, TMDs have wide application in lubrication, catalysis, energy storage, and photovoltaics.[7] In particular, a number of recent research studies on TMDs put emphasis on their electrocatalytic activity for the hydrogen evolution reaction (HER).[8] However, 2D nanomaterials display a strong tendency to restack and condense, which leads to a decrease of performance in their applications.[9] A reported method to improve the performance of 2D nanomaterials is making the 2D nanomaterials assemble to three-dimensional (3D) structures, which could combine the superiority of both nanostructures and microstructures.[10]

A general method for synthesis of hierarchical TMD nanostructures has rarely been reported.[10a] The most commonly used method for preparation of TMDs is chemical vapor deposition (CVD), which always needs high temperature, dangerous gases (H_2 and H_2S), and a complicated procedure.[11] Moreover, the low productivity of the CVD method makes them unsuitable for large-scale applications. The most promising route for the large-scale production of TMDs is a solution-phase method,[12] due to its simplicity for bulk production. However, until now, most existing solution-phase methods also needed high temperatures to obtain good crystallization structure.[8a,13] Controllable synthesis of TMDs hierarchical structures at low temperature still remains as a great challenge. A strategy to decrease the reaction temperature is the search for different precursor. As we all know, polyoxometalates (POMs) are predominantly molybdates and tungstates with well-defined structural frameworks.[14] In addition, the substitution of sulfur for oxygen in the POMs has been achieved.[15] Even more, the direct exchange of sulfur for oxygen contributes to the breaking of the polynuclear structure and the formation of TMDs.[16] More importantly, most of the substitution can occur at a lower temperature,[15] which can be in favor of the synthesis of TMDs at low-temperature. Therefore, POMs might be a good choice as the precursor.

Here we report the synthesis of TMDs by using POMs as tungsten or molybdenum precursors. Hierarchical TMDs with novel structures can be formed below 200 °C, including WS_2 rods, MoS_2 rods, and $MoSe_2$ hollow spheres. All of these hierarchical structures assembled from the corresponding nanosheets. Meanwhile the epitaxial growth of noble metal nanoparticles (NPs) on TMDs could be achieved very easily. The obtained Pt/WS_2 and Pt/MoS_2 hybrids were highly active and durable HER catalysts. Furthermore, the Pt NPs on the surface of TMDs could improve the HER activity sharply, which was likely due to the synergistic effect between Pt NPs and MoS_2 rods.

The hierarchical TMDs were synthesized by a solution-phase reaction. By using POMs and thioacetamide or selenium dioxide as precursors and n-octylamine and ethanol as solvents, crystalline TMDs were facilely obtained at 180–190 °C. First,

[a] *P. He, H. Li, H. Liu, Prof. X. Wang*
Department of Chemistry
Tsinghua University
Beijing, 100084 (China)
E-mail: wangxun@mail.tsinghua.edu.cn

Supporting information for this article is available on the WWW under http://dx.doi.org/10.1002/cnma.201500188.

This manuscript is part of a Special Issue on Nanomaterials for Energy Conversion and Storage. A link to the Table of Contents will appear here once the Special Issue is assembled.

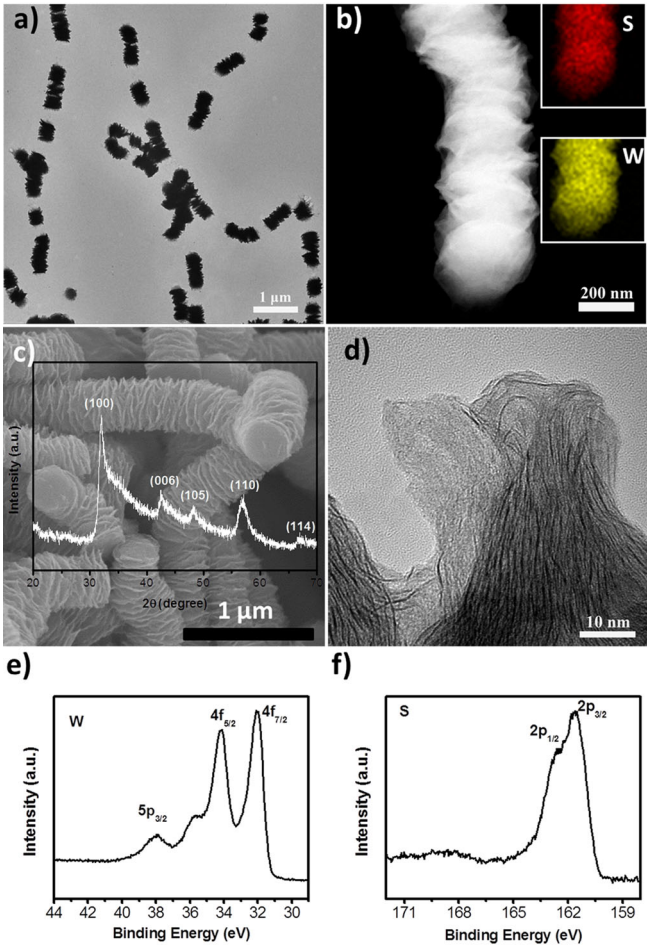

Figure 1. The characterization of the hierarchical WS_2 rods. a) TEM image, and b) STEM image (Inset: corresponding EDX mapping images) of the hierarchical WS_2 rods. c) SEM image of the WS_2 rods (Inset: the corresponding XRD pattern). d) HRTEM image of part of a WS_2 rod. XPS spectra of e) W 4f and 5p peaks, and f) S 2p peaks.

WS_2 rods were obtained when the precursors were phosphotungstic acid and thioacetamide. The morphology of the product was determined by transmission electron microscopy (TEM) and scanning electron microscopy (SEM) (Figure 1a and 1c, low-magnification SEM image is shown in Figure S1 in the Supporting Information). The low-magnification TEM image shows the platelike structure of the WS_2 rod. From the dark-field scanning transmission electron microscopy (STEM), a more dimensional layered structure can be observed (Figure 1b). At the same time, high-resolution TEM (HRTEM) imaging (Figure 1d) indicated that every layer in the SEM image (Figure 1c) consisted of numerous WS_2 nanosheets. Therefore, we think a new kind of WS_2 rod with a hierarchical structure has been obtained. An energy-dispersive X-ray (EDX) spectrum (Figure S2) and EDX mapping images (the inset in Figure 1b) confirmed the existence of tungsten and sulfur. The X-ray photoelectron spectra (XPS) of tungsten display peaks at 32 eV (W $4f_{7/2}$) and 34 eV (W $4f_{5/2}$) which are characteristic of the W^{4+} of 2H-WS_2, and the binding energies at 162 and 163 eV are features of the S^{2-} of WS_2. Furthermore, the X-ray powder diffraction (XRD) pattern (the inset in Figure 1c) of the WS_2 rods corresponds to the reference.[8a] So, we confirmed the WS_2 rods were hexagonal 2H-WS_2 phase without impurity. The apparent asymmetry of the (100) peak demonstrated we obtained a turbostratically disordered layered WS_2 rod.[8a] This result was in accord with the appearance of WS_2 rod, which was observed by HRTEM (Figure 1d).

According to the literature,[8a,17] when WCl_6[8a,17a] or $(NH_4)_{10}W_{12}O_{41}$[17b] was used as the tungsten precursor, a higher temperature above 220 °C was necessary for the formation of WS_2 nanostructures. Therefore, the POMs appear to be prerequisite for the growth of WS_2 rods at a lower temperature. We have used $Na_3PW_{12}O_{40}$ as precursor to replace the $H_3PW_{12}O_{40}$. Some white precipitates occurred after the solvothermal method. Through the TEM characterization, we found the precipitates were composed of irregular structures (Figure S3a). As Figure S3b shows, the XRD pattern showed the precipitates were not WS_2. When H_2WO_4 was used instead of $H_3PW_{12}O_{40}$, only some irregular structures were obtained (Figure S4a), and the XRD pattern (Figure S4b) indicated these nanostructures were not WS_2. On the basis of the control experiments, we deduced that the POMs affect the formation of WS_2 rods through the following aspects: (1) The strong acidic environment of POMs is indispensable for the formation of WS_2 rods at a lower temperature, because the hydrogen ion could react with thioacetamide to produce H_2S gas in the autoclave[18] and H_2S is more reactive than the thioacetamide. Finally, the H_2S reacted with the tungsten precursor to form the WS_2 at a lower temperature. When the H^+ in the $H_3PW_{12}O_{40}$ was replaced by Na^+, WS_2 phase could not form under the same conditions. This result further proves our reasoning that hydrogen ion has a great impact on the formation of WS_2. (2) The $[PO_4]^{3-}$ also plays an important role in the formation of WS_2. In the autoclave, the consumption of hydrogen ions, the existence of n-octylamine and the higher temperature (190 °C) are conducive to the departure of the $[PO_4]^{3-}$ group. Once the $[PO_4]^{3-}$ group left from the center of POMs, the polynuclear structure of Keggin-type POM was destroyed and the connectivity between the octahedron structure of $[WO_6]$ could be decreased. As Figure 2 shows, the octahedron structure of $[WO_6]$ in the POMs

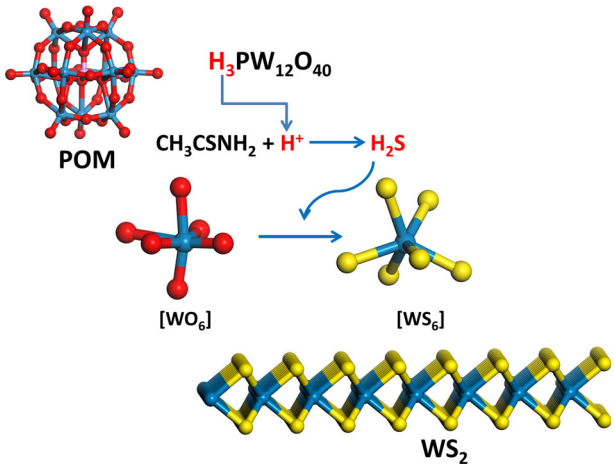

Figure 2. Scheme of the transformation from POMs to WS_2.

could allow for the formation of $[WS_6]$ structure through slight adjustment of their crystal structure. The control experiment that used H_2WO_4 instead of POMs could prove the importance of $[PO_4]^{3-}$ group in the formation of WS_2 at a lower temperature.

To further verify our theory, phosphomolybdic acid was used as precursor. Then MoS_2 rods were obtained by the same method except phosphotungstic acid was replaced by phosphomolybdic acid. A detailed explanation is given in the Experimental Section. The crystalline MoS_2 rods were formed at 180 °C in 2 hrs. The morphology of products was characterized by TEM, which revealed that the obtained samples had a rod morphology with diameters of about 150–300 nm and a length of several micrometers (Figure 3a). We also observed the layered structure of this rod. The structure of these rods was further characterized by SEM (Figure 3b). The SEM result confirmed the rods were solid construction and formed by self-assembly of MoS_2 nanosheets, and the MoS_2 layers were clearly visible in the dark-field STEM image (Figure 3c). EDX mapping analysis (the inset in Figure 3c) confirmed the even distribution of molybdenum and sulfur along the rods, and the EDX spectrum is shown in Figure S5. The HRTEM images (Figure S6) of the rim of a rod suggested some layered structure and lattice fringe. The layer spacing below 0.7 nm confirmed the single-layer character. In addition, there was no (002) diffraction in the XRD pattern (Figure S7), which further indicated the MoS_2 rod was formed by self-assembly of MoS_2 nanosheets.[9b] The XPS was used to study the chemical state of Mo and S in the rod structure (Figure S8). The XPS spectra of molybdenum displays peaks at 229 eV (Mo $3d_{5/2}$) and 232 eV (Mo $3d_{3/2}$) which are characteristic of the Mo^{4+} of MoS_2, and the binding energies at 162 and 163 eV are features of the S^{2-} of MoS_2.[10a]

By using phosphotungstic acid and selenium dioxide as precursors, $MoSe_2$ hollow spheres were obtained at 180 °C. The detailed description is also given in the Experimental Section. The morphology of the sample has been studied by SEM (Figure S9) which shows the products have elliptical sphere structures with a size of 150–200 nm. From the low-magnification TEM image (Figure 3d), we could observe the inner hollow sphere structure. The hollow structure was also more visible in the dark-field STEM image (Figure 3e). The EDX mapping (the insets in Figure 3e) confirmed the even distribution of molybdenum and selenium, and the EDX line-scan (Figure 3f) analysis confirmed the products are elliptical hollow spheres. The $MoSe_2$ hollow spheres also have been characterized by HRTEM. The HRTEM image (Figure S10a) of the rim of a sphere showed some layered structure, and the lattice fringe could be observed in Figure S10b at the rim. Therefore, we can conclude the hierarchical $MoSe_2$ hollow spheres was formed by the self-assembly of $MoSe_2$ nanosheets. The XRD pattern of this product is shown in Figure S11. We think the difference of chalcogenide precursors (sulfur source: CH_3CSNH_2 and selenium source: SeO_2) led to the difference in structures of $MoSe_2$ and MoS_2.

Both the successful synthesis of MoS_2 rods and $MoSe_2$ hollow spheres proves the POMs are a new kind of precursors for the formation of TMDs. Meanwhile, these results gave a basis for our reasoning that the hydrogen ion and $[PO_4]^{3-}$ played important roles in the formation of the hierarchical

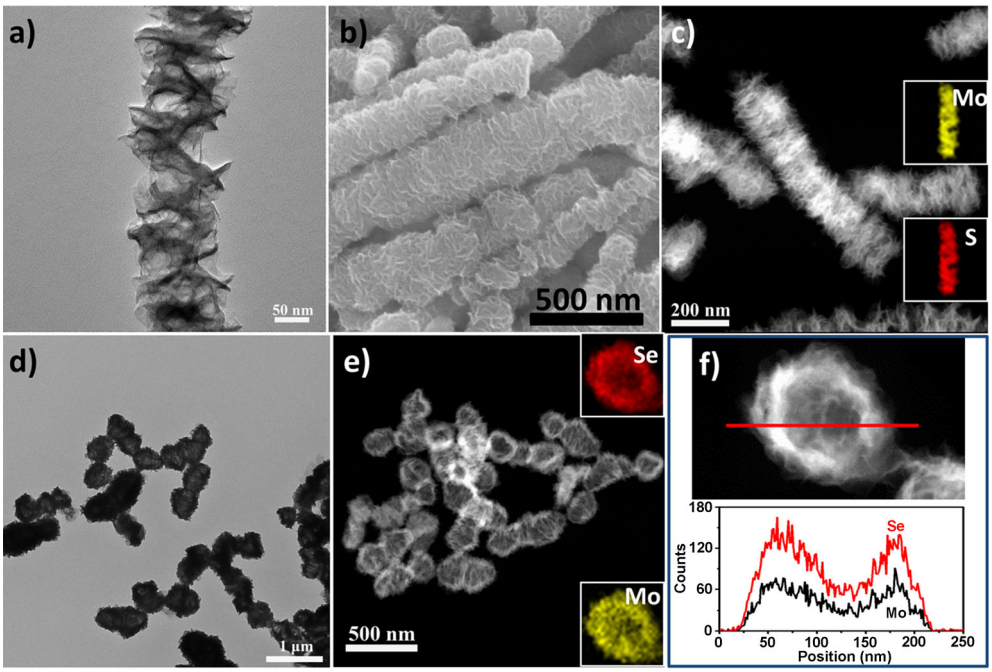

Figure 3. Characterization data of hierarchical MoS_2 rods and $MoSe_2$ hollow spheres. a) TEM image, b) SEM image, and c) STEM image (Inset: corresponding EDX mapping images) of the MoS_2 rods. d) TEM image, e) STEM image (Inset: corresponding EDX mapping images), f) EDX profile scanning result of the $MoSe_2$ hollow spheres.

TMDs. Therefore, we think it is possible to expand our current strategy to other POMs with phosphate group and hydrogen ion as cation.

In order to extend the application of these TMDs, epitaxial growth of noble metal (palladium or platinum) on WS_2 rods and MoS_2 rods has been achieved. The NPs were synthesized in situ on the surface of WS_2 rods or MoS_2 rods. $PdCl_2$ or H_2PtCl_6 were used as metal precursors and different reductants were used (see the detailed method in the Experimental Section). For example, Pd NPs were synthesized on WS_2 rods by reduction of $PdCl_2$ with polyvinylpyrrolidone (PVP). As shown in the TEM image in Figure S12, Pd NPs with diameter of about 5 nm were on WS_2 rods or MoS_2 rods, which indicated the epitaxial growth of Pd NPs on TMDs surface. When the H_2PtCl_6 was reduced by HCHO, Pt NPs on the surface of WS_2 rods or MoS_2 rods could be obtained. Pt NPs with size of about 5 nm epitaxially grew on the surface of WS_2 rods (Figure 4a). As shown in the SEM image in Figure S13a, the Pt NPs

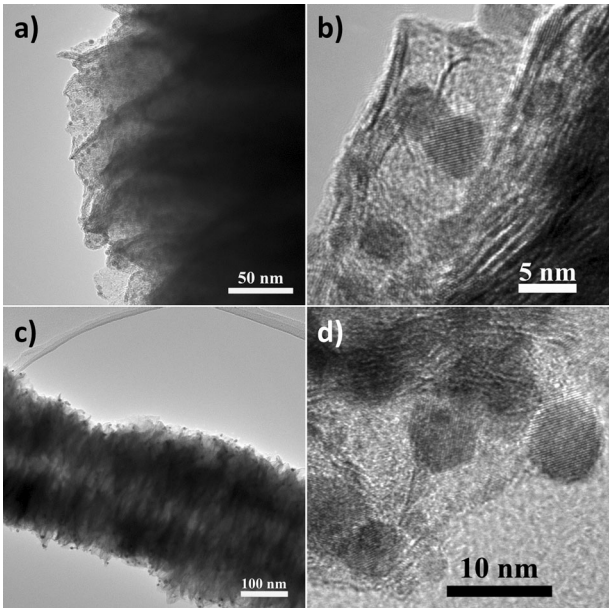

Figure 4. a) TEM image, and b) HRTEM image of the Pt/WS_2 hybrid. c) TEM image, and d) HRTEM image of the Pt/MoS_2 hybrid.

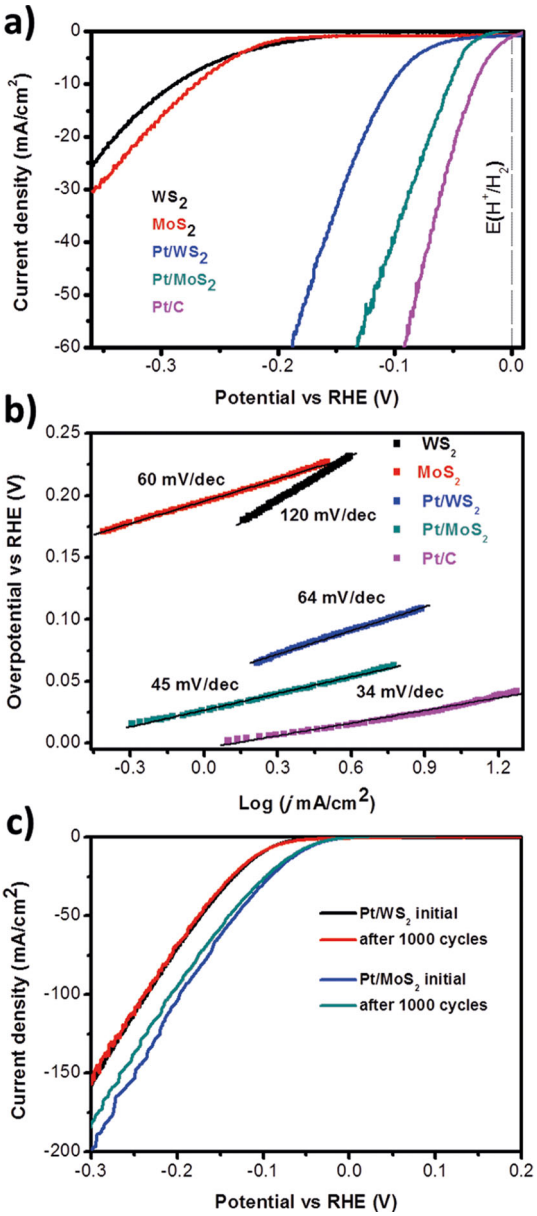

Figure 5. HER performance of the samples. a) Polarization curves of WS_2, MoS_2, Pt/WS_2, Pt/MoS_2, and Pt/C. b) Tafel plots of the corresponding samples. LSV curves for c) Pt/WS_2 hybrid and Pt/MoS_2 hybrid samples in 0.5 M H_2SO_4 initially and after 1000 CV sweeps between +0.2 V and −0.3 V versus RHE.

on the surface of WS_2 rods were also visible. HRTEM analysis was carried out on the Pt/WS_2 hybrid structures (Figure 4b). Similar with the Pt/WS_2, most of the 5 nm Pt NPs also grew on the MoS_2 surface (Figure 4c). The Pt/MoS_2 hybrid structures also have been characterized by HRTEM (Figure 4d). EDX mapping of Pt/WS_2 (Figure S14a) and Pt/MoS_2 (Figure S14b) hybrid structures confirmed the even distribution of platinum, sulfur, tungsten, or molybdenum. The STEM images of Pt/WS_2 and Pt/MoS_2 are shown in Figure S14.

The Pt/WS_2 and Pt/MoS_2 hybrid structures should be high-efficiency catalysts for the HER. This kind of hybrid structures can be produced in large amounts, which is favorable for their applications. In order to compare the electrocatalytic activity between WS_2 rods, MoS_2 rods, Pt/WS_2 hybrids (9.4 wt% Pt in Pt/WS_2 hybrid), Pt/MoS_2 hybrids (8.6 wt% Pt in Pt/MoS_2 hybrid), and the commercial Pt/C catalyst (20% Pt in Pt/C), the HER activity of these five catalysts have been tested. As shown in Figure 5a and 5b, both the synthesized WS_2 rods and MoS_2 rods exhibit undistinguished HER catalytic activities, and the Pt/C shows the best HER activity with negligible overpotential.[19] The Pt/WS_2 and Pt/MoS_2 hybrids exhibited excellent electrocatalytic activities towards HER with overpotentials less than 100 mV. The Pt/MoS_2 hybrids showed the superior HER activity with a much smaller onset potential of ≈35 mV and higher catalytic current, while pure MoS_2 rods exhibited inferior HER activity with a larger onset potential of ≈230 mV. Therefore, the epitaxial growth of Pt NPs on TMDs could remarkably in-

crease the HER activity. The HER kinetics of the WS_2, MoS_2, Pt/WS_2, Pt/MoS_2, and Pt/C were probed by the Tafel plots (log j–η) (Figure 5b). Tafel slope of ≈45 mV per decade was measured for Pt/MoS_2 hybrids, which was lower than that of ≈60 mV per decade for MoS_2 rods and close to the value of ≈34 mV per decade for Pt/C catalyst. Similarly, Tafel slope of ≈64 mV per decade for Pt/WS_2 was lower than that of ≈120 mV per decade for WS_2 rods. According to the reference,[8c,20] these Tafel slopes suggest a Volmer–Heyrovsky mechanism works in the catalyst of WS_2 rods, MoS_2 rods, Pt/WS_2 and Pt/MoS_2 hybrids. To study the durability of the Pt/WS_2 and Pt/MoS_2 hybrid, the LSV curves of Pt/WS_2 and Pt/MoS_2 hybrid catalyst before and after 1000 potential cycles are shown in Figure 5c. For the Pt/WS_2 and Pt/MoS_2 hybrids, there was no obvious shift in the polarization curves. We have also examined the morphology of Pt/WS_2 and Pt/MoS_2 hybrids under TEM observation after continuous linear potential sweeps in 0.5 M H_2SO_4 (Figure S15). The nanostructures were well-retained during the electrocatalytic reaction. These results indicated the catalytic stability of Pt/WS_2 and Pt/MoS_2 hybrids could be kept after long-term use. In addition, XPS was used to study the valence state of Pt in the hybrid nanomaterials (Figure S16). The binding energies at 71.9 eV ($4f_{7/2}$) and 75 eV ($4f_{5/2}$) indicated the electron transferred from the Pt NPs to the TMDs.[21]

In summary, we have developed a low-temperature, solution-phase method for the synthesis of 3D hierarchical TMDs. Hierarchical WS_2 rods, MoS_2 rods, and $MoSe_2$ hollow spheres based on self-assembly of the corresponding single-layer nanosheets were obtained by using POMs as tungsten or molybdenum precursors below 200 °C. The POMs appear to be prerequisite for the formation of hierarchical TMDs at a lower temperature. Therefore, the hydrogen ion and $[PO_4]^{3-}$ group played important roles in the formation of the hierarchical TMDs. At the same time, the epitaxial growth of noble metal (palladium or platinum) NPs on WS_2 and MoS_2 rods has been achieved. The Pt/MoS_2 hybrids in all the samples we tested (WS_2 rods, MoS_2 rod, Pt/WS_2, and Pt/MoS_2) shows the best HER activity with onset potential of ≈35 mV, which approaches the performance of Pt/C catalyst. We believe that our study will facilitate the synthesis of hierarchical TMDs at low temperature.

Experimental Section

Synthesis of WS_2 rods

120 mg phosphotungstic acid [$H_3PW_{12}O_{40}$·$x$$H_2O$] and 91 mg thioacetamide were added into 4 mL n-octylamine and 1 mL ethanol. Then this solution was transferred to a 10 mL autoclave and heated at 190 °C for 12 hrs. After the reaction, the product was washed with cyclohexane and ethanol through centrifugation for three times.

Control experiments

123 mg $Na_3PW_{12}O_{40}$ (or 125 mg H_2WO_4) and 91 mg thioacetamide were added into 4 mL n-octylamine and 1 mL ethanol. Then this solution was transferred to a 10 mL autoclave and heated at 190 °C for 12 hrs. After the reaction, the product was washed with cyclohexane and ethanol through centrifugation for three times.

Synthesis of MoS_2 rods

0.5 mL of phosphomolybdic acid (ethanol, 0.042 M) and 0.5 mL of thioacetamide (ethanol, 1.19 M) were added to 2 mL n-octylamine and 2 mL ethanol. Then this solution was transferred to a 10 mL autoclave and heated at 180 °C for 2 hrs. After the reaction, the product was washed with cyclohexane and ethanol through centrifugation for three times.

Synthesis of $MoSe_2$ hollow spheres

38 mg phosphomolybdic acid [$H_3PMo_{12}O_{40}$·$x$$H_2O$] and 56 mg SeO_2 were added into 3 mL n-octylamine and 2 mL ethanol. Then this solution was transferred to a 10 mL autoclave and heated at 180 °C for 12 hrs. After the reaction, the product was washed with cyclohexane and ethanol through centrifugation for three times.

Synthesis of Pd/WS_2 and Pd/MoS_2 hybrids

1 mL of the WS_2 dispersion (0.05 mmol W in 1 mL formamide) and 4 mL formamide was mixed. Then, 0.2 g PVP (MW 8000) and 10 mg $PdCl_2$ were added sequentially. Then the autoclave was sealed and heated at 130 °C for 4 hrs. After the reaction, the product (Pt/WS_2 hybrid) was washed with ethanol through centrifugation for three times. The Pd/MoS_2 hybrids were obtained by the same method.

Synthesis of Pt/WS_2 and Pt/MoS_2 hybrids

1 mL of the WS_2 dispersion (0.05 mmol W in 1 mL formamide) and 4 mL formamide was mixed. Then, 1 mL formaldehyde solution and 60 μL H_2PtCl_6 solution (aqueous, 0.029 M) were added sequentially. Then the autoclave was sealed and heated at 130 °C for 4 hrs. After the reaction, the product (Pt/WS_2 hybrid) was washed with ethanol through centrifugation for three times. The Pt/MoS_2 hybrids were obtained by the same method.

Sample preparation and electrochemical characterization

5 mg of the catalyst was dispersed in 950 μL of ethanol, and 50 μL of 5 wt% Nafion solution. And the mixed solution was sonicated for 30 min to form a homogeneous ink. Then 6 μL of the ink (loading about 30 μg of the catalyst) was loaded on a glassy carbon electrode as working electrode with a rotating speed of 1600 rpm. The measurements were performed in 0.5 M H_2SO_4 solution using a standard three-electrode system, with a graphite rod counter electrode and a Hg/HgO reference electrode. The reference electrode was calibrated and converted to reversible hydrogen electrode (RHE). Linear sweep voltammetry (LSV) was carried out at 5 mV s^{-1} after the catalyst was cycled more than 50 times by cyclic voltammetry (CV).

Acknowledgements

This work was supported by NSFC (21431003, 91127040, 21221062), and the State Key Project of Fundamental Research for Nanoscience and Nanotechnology (2011CB932402).

Keywords: hierarchical · low-temperature · polyoxometalate · solution-phase · tungsten disulfide

[1] a) K. S. Novoselov, V. I. Falko, L. Colombo, P. R. Gellert, M. G. Schwab, K. Kim, *Nature* **2012**, *490*, 192–200; b) N. Tombros, C. Jozsa, M. Popinciuc, H. T. Jonkman, B. J. van Wees, *Nature* **2007**, *448*, 571–574.

[2] a) R. Raccichini, A. Varzi, S. Passerini, B. Scrosati, *Nat. Mater.* **2015**, *14*, 271 – 279; b) J. Xu, K. Wang, S.-Z. Zu, B.-H. Han, Z. Wei, *ACS Nano* **2010**, *4*, 5019 – 5026.
[3] a) Y. Xu, G. Shi, X. Duan, *Acc. Chem. Res.* **2015**, *48*, 1666 – 1675; b) T. Ramanathan, A. A. Abdala, S. Stankovich, D. A. Dikin, M. Herrera Alonso, R. D. Piner, D. H. Adamson, H. C. Schniepp, ChenX, R. S. Ruoff, S. T. Nguyen, I. A. Aksay, R. K. Prud'Homme, L. C. Brinson, *Nat. Nanotechnol.* **2008**, *3*, 327 – 331.
[4] F. Xia, D. B. Farmer, Y.-m. Lin, P. Avouris, *Nano Lett.* **2010**, *10*, 715 – 718.
[5] M. Chhowalla, H. S. Shin, G. Eda, L.-J. Li, K. P. Loh, H. Zhang, *Nat. Chem.* **2013**, *5*, 263 – 275.
[6] a) P. Johari, V. B. Shenoy, *ACS Nano* **2012**, *6*, 5449 – 5456; b) X. Huang, Z. Zeng, H. Zhang, *Chem. Soc. Rev.* **2013**, *42*, 1934 – 1946.
[7] a) H. Li, J. Wu, Z. Yin, H. Zhang, *Acc. Chem. Res.* **2014**, *47*, 1067 – 1075; b) Q. H. Wang, K. Kalantar-Zadeh, A. Kis, J. N. Coleman, M. S. Strano, *Nat. Nanotechnol.* **2012**, *7*, 699 – 712; c) D. Kong, J. J. Cha, H. Wang, H. R. Lee, Y. Cui, *Energy Environ. Sci.* **2013**, *6*, 3553 – 3558.
[8] a) L. Cheng, W. Huang, Q. Gong, C. Liu, Z. Liu, Y. Li, H. Dai, *Angew. Chem. Int. Ed.* **2014**, *53*, 7860 – 7863; *Angew. Chem.* **2014**, *126*, 7994 – 7997; b) J. Duan, S. Chen, B. A. Chambers, G. G. Andersson, S. Z. Qiao, *Adv. Mater.* **2015**, *27*, 4234 – 4241; c) M.-R. Gao, J.-X. Liang, Y.-R. Zheng, Y.-F. Xu, J. Jiang, Q. Gao, J. Li, S.-H. Yu, *Nat. Commun.* **2015**, *6*, 5982; d) S. Chen, J. Duan, Y. Tang, B. Jin, S. Z. Qiao, *Nano Energy* **2015**, *11*, 11 – 18; e) Y. Jiao, Y. Zheng, M. Jaroniec, S. Z. Qiao, *Chem. Soc. Rev.* **2015**, *44*, 2060 – 2086.
[9] a) K. Chang, W. Chen, L. Ma, H. Li, H. Li, F. Huang, Z. Xu, Q. Zhang, J.-Y. Lee, *J. Mater. Chem.* **2011**, *21*, 6251 – 6257; b) X. Yang, J. Zhu, L. Qiu, D. Li, *Adv. Mater.* **2011**, *23*, 2833 – 2838.
[10] a) P.-p. Wang, H. Sun, Y. Ji, W. Li, X. Wang, *Adv. Mater.* **2014**, *26*, 964 – 969; b) Z. Tang, S. Shen, J. Zhuang, X. Wang, *Angew. Chem. Int. Ed.* **2010**, *49*, 4603 – 4607; *Angew. Chem.* **2010**, *122*, 4707 – 4711; c) J. S. Chen, Y. L. Tan, C. M. Li, Y. L. Cheah, D. Luan, S. Madhavi, F. Y. C. Boey, L. A. Archer, X. W. Lou, *J. Am. Chem. Soc.* **2010**, *132*, 6124 – 6130; d) L. Zhang, H. B. Wu, Y. Yan, X. Wang, X. W. Lou, *Energy Environ. Sci.* **2014**, *7*, 3302 – 3306.
[11] a) S. Zhuo, Y. Xu, W. Zhao, J. Zhang, B. Zhang, *Angew. Chem. Int. Ed.* **2013**, *52*, 8602 – 8606; *Angew. Chem.* **2013**, *125*, 8764 – 8768; b) M. Nath, A. Govindaraj, C. N. R. Rao, *Adv. Mater.* **2001**, *13*, 283 – 286.
[12] W. Jung, S. Lee, D. Yoo, S. Jeong, P. Miró, A. Kuc, T. Heine, J. Cheon, *J. Am. Chem. Soc.* **2015**, *137*, 7266 – 7269.
[13] S. Jeong, D. Yoo, J.-t. Jang, M. Kim, J. Cheon, *J. Am. Chem. Soc.* **2012**, *134*, 18233 – 18236.
[14] M. T. Pope, A. Müller, *Angew. Chem. Int. Ed. Engl.* **1991**, *30*, 34 – 48; *Angew. Chem.* **1991**, *103*, 56 – 70.
[15] E. Cadot, M. N. Sokolov, V. P. Fedin, C. Simonnet-Jegat, S. Floquet, F. Secheresse, *Chem. Soc. Rev.* **2012**, *41*, 7335 – 7353.
[16] M. N. Sokolov, I. V. Kalinina, E. V. Peresypkina, E. Cadot, S. V. Tkachev, V. P. Fedin, *Angew. Chem. Int. Ed.* **2008**, *47*, 1465 – 1468; *Angew. Chem.* **2008**, *120*, 1487 – 1490.
[17] a) B. Mahler, V. Hoepfner, K. Liao, G. A. Ozin, *J. Am. Chem. Soc.* **2014**, *136*, 14121 – 14127; b) Q. Liu, X. Li, Z. Xiao, Y. Zhou, H. Chen, A. Khalil, T. Xiang, J. Xu, W. Chu, X. Wu, J. Yang, C. Wang, Y. Xiong, C. Jin, P. M. Ajayan, L. Song, *Adv. Mater.* **2015**, *27*, 4837 – 4844.
[18] E. H. Swift, E. A. Butler, *Anal. Chem.* **1956**, *28*, 146 – 153.
[19] Y. Zheng, Y. Jiao, S. Z. Qiao, *Adv. Mater.* **2015**, *27*, 5372 – 5378.
[20] a) B. E. Conway, B. V. Tilak, *Electrochim. Acta* **2002**, *47*, 3571 – 3594; b) J. Duan, S. Chen, M. Jaroniec, S. Z. Qiao, *ACS Nano* **2015**, *9*, 931 – 940; c) Y. Zheng, Y. Jiao, M. Jaroniec, S. Z. Qiao, *Angew. Chem. Int. Ed.* **2015**, *54*, 52 – 65; *Angew. Chem.* **2015**, *127*, 52 – 66.
[21] X. Huang, Z. Zeng, S. Bao, M. Wang, X. Qi, Z. Fan, H. Zhang, *Nat. Commun.* **2013**, *4*, 1444.

Manuscript received: October 31, 2015
Accepted Article published: November 11, 2015
Final Article published: ■■ ▮▮, 0000

COMMUNICATION

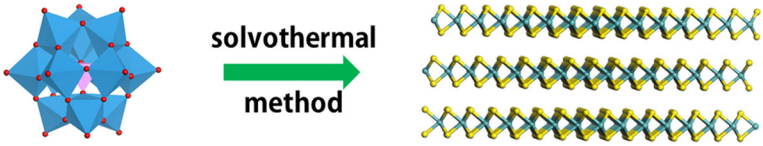

Hierarchical transition metal dichalcogenides (TMDs) with novel structures can be formed below 200 °C, including WS_2 rods, MoS_2 rods, and $MoSe_2$ hollow spheres, by using polyoxometalates (POMs) as tungsten or molybdenum precursors. The epitaxial growth of noble metal nanoparticles on TMDs could be achieved, and the obtained Pt/WS_2 and Pt/MoS_2 hybrids were highly active and durable hydrogen evolution reaction (HER) catalysts.

2D Materials

*Peilei He, Haoyi Li, Huiling Liu, Xun Wang**

■■ – ■■

Generalized Synthesis of Hierarchical Transition Metal Dichalcogenide Nanosheets from Polyoxometalates